Fermi National Accelerator Laboratory

FERMILAB-FN-570

Depth Requirements in SSC Calorimeters

D. Green, A. Beretvas, K. Denisenko, N. Denisenko, J. Marraffino, A. Para, and W. Wu

Fermi National Accelerator Laboratory
P.O. Box 500, Batavia, Illinois 60510

August 1991

Operated by Universities Research Association Inc. under contract with the United States Department of Energy

DEPTH REQUIREMENTS IN SSC CALORIMETERS

The FNAL SDC Simulation Group
(D. Green, A. Beretvas, K. Denisenko,
N. Denisenko J. Marraffino, A. Para, W. Wu)
Fermilab

1. Introduction

The depth requirements for a calorimeter to be used at the SSC are herein explored. Obviously, this parameter is a crucial cost driving element as it defines the size of the muon system, and the materials cost of the calorimeter itself. For this reason, it is imperative to make the calorimeter depth as shallow as possible. Balancing this tendency, the depth must be of a sufficient thickness so as not to compromise a variety of Physics issues. Among those topics are jet energy resolution, the size of the cross section for missing transverse momentum, and the filtering of hadrons before they enter the muon system.

2. Longitudinal Leakage in Calorimeters

The first task to be accomplished is to collect data on longitudinal leakage and leakage fluctuations in calorimeters. This data could then be parametrized and the parameterization used in a Monte Carlo program. It was thought to be important to use an ensemble of data sets since they would differ in energy range, beam tagging, transverse containment, longitudinal containment, and perhaps other systematic factors.

It is also true that in extrapolating to the SSC one must go beyond the region of validity of the data. A variety of functional fits allows one some idea of the systematic errors in this case.

2.1 CITF Model

As a first step, the data from the CITF collaboration[1] are parameterized so as to make a model to extrapolate to all energies. Some of the data are shown in Fig. 1. The approximation is made that the fluctuation in the contained energy fraction f, scaling as $\sqrt{f}$, causes a degradation in energy resolution, r =

dE(f)/dE(1), which is energy independent. It is further assumed that the depth of absorber needed for a containment fraction f scales logarithmically with the incident energy E, see Fig. 1b. This assumption is obvious, given the general properties of hadronic showers.[2] The parameterization given below, Eq. 1, is shown as dashed curves in Fig. 1. The energy, E, is in GeV units.

$$\begin{aligned} (1-1/r) &= a\sqrt{1-f} \\ D &= D_0 \exp(-b\sqrt{1-f}) \\ D_0 &= c + d\ln E. \end{aligned} \qquad (1)$$

The parameters are, a = 0.9, b = 3.2, d = 0.43, and c = 3.51 absorption lengths in steel. Note that in what follows, an absorption length is defined to be 16.76 cm of steel. This form provides a reasonable representation of the data given in Fig. 1. Shown in Fig. 2 is the value of r as a function of depth at fixed energy. Again the parameterization given in Eq. 1 works fairly well. Other data sets have been checked against this formulation. A data set spanning the same energy range is well represented by the f = 0.95 curve analogous to those data shown in Fig. 1b.[3] Similarly, the curve analogous to Fig. 2 is well represented at lower energies.[4] However, as a note of caution, some data[5] for r as a function of E are not well matched to Eq. 1, at least at energies above 100 GeV.

2.2 WA1 Model

The form given above will be used in all the work which follows. It is convenient for hand calculations and for incorporation into Monte Carlo simulations. Note, however, that this formulation represents only the Gaussian part of the error. There is a long asymmetric tail which has not been parameterized. In order to answer this objection to the model and to obtain an ensemble of data sets a second form was also studied. Having several forms allows one to check that the conclusions are stable under variations of the input assumptions. This second model uses an averaged shower shape.[6]

$$dE = c_1\, fo\, t^{a-1} e^{-bt} dt + c_2 (1 - fo) D^{a-1} e^{-gD} dD. \qquad (2)$$

The energy has an electromagnetic, (fo), and an hadronic, (1 - fo), component. The depth is in radiation length, t, units and absorption length, D = $\lambda/\lambda o$, units. The normalization is, $c_1 = Eb^a/\Gamma(a)$ and $c_2 = Eg^a/\Gamma(a)$.

Assuming that the electromagnetic energy is rapidly absorbed, the hadronic energy fraction leakage from a depth v = gD, $\Delta E/E$, and the corresponding energy error (using an asymptotic expansion), dE/E, due to fluctuations in electromagnetic fraction, dfo, and conversion point, dD, is,

$$\begin{aligned} \Delta E/E &= -(1-fo)\,\Gamma(a,v)/\Gamma(a) \\ dE/E &\sim (\Delta E/E)(1/[1-fo])\,dfo \oplus [-1+(a-1)/v]\,dD. \end{aligned} \tag{3}$$

In Eq. 3 $\Gamma(a,v)$ is the incomplete gamma function and only the first term in an asymptotic expansion has been retained in estimation the error. Using the parameters a, b, g, and fo given in Ref. 6, this form was checked against the form given in Eq. 1a, i.e. is f = $\Delta E/E$? The agreement is quite good. The advantage of this second scheme is that the fluctuations in the hadron conversion point, dD, and in the electromagnetic fraction, dfo, will lead to an asymmetric distribution in $\Delta E/E$ and hence to a tail in the resolution dE due to the fluctuations in ΔE. In Eq. 3 only the Gaussian error is quoted.

2.3 CDHS Model

A third technique uses the data on resolution due to leakage given by the CDHS group.[7] A reasonable representation of the data, after deconvoluting the calorimeter resolution itself, is

$$\begin{aligned} (dE/E) &= 1.6\,e^{-(D/D_{EFF})} \\ D_{EFF} &= 0.93\,(1+0.49\ln E). \end{aligned} \tag{4}$$

Thus, at any depth D, for any energy E, one can find the effective interaction length D_{EFF}, and then the leakage contribution to the energy resolution.

For example, at 1.0 TeV, for a depth, D, of 10, D_{EFF} = 4.08 and (dE/E) due to leakage is 14%. By comparison, using Eq. 1, the first method yields D_o = 13.94. Since the first two methods have depths referred to the interaction point (Eq. 1, Eq. 2), while the third method refers to the physical calorimeter depth, roughly 1 absorption length should be removed in comparing Eq. 1 to Eq. 4. Thus, D = 9 in Eq. 1, the containment factor f is 0.98, and r = 1.14. Since r refers to the ratio of resolution with respect to $dE(1) \equiv 1.1/\sqrt{E} \oplus 0.03 = 0.046$, the deconvoluted leakage error is (dE/E) 2.5%. At first glance, these two formulations do not seem to be compatible.

In fact, the discrepancy is only apparent. The CDHS fit uses rms for a distribution which is distinctly not a Gaussian. We have compared the data of Sections 2.3 and 2.4 analyzed in comparable ways and convinced ourselves that no contradiction exists. That being the case, we drop reference to the CDHS model in what follows since we do not have available a convenient Gaussian fit to be parametrized.

2.4 Lab E Model

In order to improve the energy range and containment properties available in the models, Lab E test beam data was used.[8] This data spans the range 15 to 450 GeV, which we will see is a range almost sufficient for the maximum transverse energy jet accessible at the SSC. The energy seen upstream of a given depth was fit to a Gaussian, and the width was characterized as in Eq. 4. Since the algorithm was different, compared to the CDHS rms calculation, the values were, therefore, rather different. The parameterization was, $dE/E = 0.5 \exp(-D/D_{EFF})$ with $D_{EFF} = 0.88 (1 + 0.35 \ln E)$. The contained energy fraction, f, was found to be well represented by the form given in Eq. 1. The values of the parameters for the Lab E data, b = 2.4, c = 5.5, and d = 0.19 result in values of D and D_0 which are compatible with those of the CITF model over the range of energies spanned by the data.

These three models were used in all subsequent work. The spread among them is an indication of the "systematic error" to be found among the existing published data on depth and energy resolution in hadron calorimeters.

3. Dijets and Depth Requirements

One possible physics topic which might drive the design of an SSC calorimeter is the measurement of dijet masses. The question to be answered is;

what is the highest possible dijet mass which can be measured at SSC design luminosity? From the answer follows the highest jet energy which must be well measured.

3.1 Maximum Accessible Mass

The question of QCD jets has been addressed many times in the context of the SSC.[9] Curves are given in Ref. 9. A rough parameterization is needed to extrapolate from these curves to the cases of interest. The simple form[10] shown below has been adopted to do this extrapolation:

$$d\sigma / dM \;=\; g(1-M/\sqrt{s})^{12} / M^{3}. \tag{5}$$

The constant g is roughly 1.2 mb $(\mathrm{GeV})^2$, M is the dijet mass, and s is the square of the CM energy. This form is an adequate representation of the exact calculation[9] for dijet transverse momenta, $P_t \sim M/2$, in the range 2 to 4 TeV. Using this form one finds that at design luminosity, in a one year, $= 10^7$ sec, run, there are ~ 150 events in a ±2% mass bin for a 10 TeV dijet mass (P_t = 5.0 TeV). Hence, one runs out of statistics at a dijet mass around 10 TeV in that the statistical error is 8% in a bin set by the 2% resolution.

3.2 Fragmentation

The next task is to make the connection between jet energy containment and the energy containment of individual hadrons. For the purposes of hand estimates and building up intuition, a simple form[11] of the jet fragmentation function, D(z), is adopted. This function specifies the probability that a jet of momentum P fragments into a hadron of momentum k; z is the momentum fraction carried off by the hadron:

$$\begin{aligned} k_i &= z_i\, P, \Sigma\, z_i = 1 \\ D(z) &= [(h+1)\,(1-z)^h]\,/\,z \\ <n> &= (h+1)\,[\ln\,(1\,/\,z_0) - (h - h[h-1]\,/\,4 + \ldots + 1\,/\,h)] \\ z_0 &= m_\pi\,/\,P. \end{aligned} \tag{6}$$

This form is a reasonable parameterization of the existing e^+e^- data[12] for the charged multiplicity if one assumes that the total multiplicity is a factor 3/2 higher and if h is ~ 6.0. This form also provides a good representation of the CDF data.[13] The shape of D(z) as a function of z is given in Fig. 3. The dashed and dashed-dotted curves are the approximate forms, $D(z) = 7/z$ and $D(z) = 125 \exp(-13z)$ respectively. Since the integral of D(z) is the multiplicity, Eq. 6, one can find the average location of particles in the fragmentation chain. The locations are also indicated in Fig. 3. For example, the "leading" fragment exists between z = 1.0 and z = 0.174. Although the fluctuations are enormous, one can assign a mean z location for the leading fragment.

$$\begin{aligned} \langle Z_1 \rangle &\sim 0.23 \\ k_t &\sim \langle z_1 \rangle P_t . \end{aligned} \tag{7}$$

This point, $\langle z_1 \rangle$, is defined to be the point where the mean multiplicity starting from the end point of z at z = 1 is = 0.5. Hence, it is the mean location of the "leading" fragment.

The estimate for $\langle z_1 \rangle$ allows us to estimate the angular scaling of an SSC detector immediately. A glance at Eq. 1 shows that, for a given containment fraction f, the required depth ratio depends only on energy and not f. Picking a fixed $P_t = 5.0$ TeV, set by the maximum accessible dijet mass, $k_t = \langle z_1 \rangle P_t$. The dependence as a function of rapidity, y, is quite weak (logarithmic). The approximate relation, $y = -\ln[\tan(\theta/2)]$ has been assumed:

$$D(y)/D(0) = (1 + d \ln[k_t/\sin\theta])/(1 + d \ln[k_t]). \tag{8}$$

The ratio is displayed in Fig. 4. Clearly there is only a minor thickness increase in the calorimetry as the result of increasing y from y = 0 to y = 3. Note that this result is independent of which value of f is ultimately deemed necessary.

3.3 Estimate, f = 0.99

As a first guesstimate, one can ask for f = 0.99 for a jet of transverse momentum P_t. As seen in Fig. 1a, this requirement would insure that the dijet mass would be well measured on the scale of the calorimeter energy error, which at high masses would be a few percent. Individual particles in the jet would be measured to 4% error or less due to leakage. Using $<z_1>$ and taking as an upper limit M = 10 TeV, one gets the curve of 99% containment depth as a function of P_t which is shown in Fig. 5. This Figure is made by assuming that the f = 0.99 criterion applies to the leading fragment. Using this criterion, one gets a very crude estimate that ~ 10 to 11 absorption lengths are required.

3.4 Mass Errors Due to Calorimeter Resolution

There are many sources of mass error. For "low" masses, 0.1 TeV and 1.0 TeV, the mass resolution is not determined by the energy measurement but by fluctuations in the jet fragmentation and in the underlying event.[14] As discussed below, at high enough mass, this will not be the case. In the equation which follows it is assumed that the vector sum of momenta is roughly the scaler sum (Eq. 6). One further assumes that, as in low P_t jets, the mass resolution is dominated by momentum errors. Finally, one assumes that the calorimeter granularity is sufficiently fine that individual hadrons are independently measured. If the calorimeter energy resolution, dE, determines the mass resolution, dM, then;

$$\begin{aligned} dE/E &= S/\sqrt{E} \oplus t \\ dM/M &\sim s/\sqrt{M} \oplus t < z_1 > /\sqrt{2}. \end{aligned} \tag{9}$$

The second formula follows from the first using Eq. 6 and propagating the errors. It is assumed that the sum of the squares of z_i can be approximated by the leading term z_1^2.

For example, a typical hadronic calorimeter resolution might be s = 0.5, t = 0.03. These values of the parameters have been used in the Monte Carlo studies described below. This single particle resolution leads to a dijet mass resolution as given in Eq. 9. The resolution, dM/M, as a function of calorimeter depth, at fixed mass = 10 TeV, is shown in Fig. 6. In this Figure, the value of r in Eq. 1 was assumed to refer to the quoted resolution of Ref. 1 folded in quadrature with a leakage term, as discussed above.

Clearly, the constraints on depth are rather soft, given the logarithmic dependence of D_0. Note that D_0 ~ 14.1 absorption lengths for the leading particle fragment. Note also that dM/M is ~ 1% at great depths which is very small on the scale of "low" mass errors.[14] Obviously, a detailed Monte Carlo is required to quantify these estimates and to elucidate the size of the fluctuations due to fragmentation, the underlying event, and the existence of heavy flavors in the jet. For this purpose, the package SSCSIM, a FNAL supported product,[15] was used.

3.5 Monte Carlo Results

There are several effects in addition to measurement error which are important to dijet mass resolution. The underlying event contains a fluctuating amount of transverse energy which may fall into a "cone" containing the jet. With a density of 8 particles per inelastic event per unit of rapidity, where each particle contains roughly 0.6 GeV of k_t, one has 4.8 GeV per unit of y. This means roughly 1.1 GeV within a cone of radius, $R = \sqrt{(\Delta y)^2 + (\Delta\phi)^2} = 0.6$ for "minbias" events. Hard scattering events have a higher density; the SSCSIM result is that there is ~ 5.0 GeV within a cone of radius R = 0.6 for 10 TeV dijet events.

The jet contains many soft fragments as shown in Fig. 3. For a cone of radius 0.7, and k_t ~ 0.6 GeV, all fragments with momenta less than k_{min} = 0.86 GeV will fall outside the cone radius and be lost. Given the form of D(z), this means that ~ $(h+1)k_{min}$ ~ 6.0 GeV falls outside the search cone. One can optimize the search cone; but a smaller size loses more fragments, while a larger size adds more extraneous underlying event energy. Thus, there is an optimal cone. In this work the magnetic field effects are not studied. Presumably, they would act so as to increase the fluctuations.

Fluctuations set a scale P_{fluc} ~ 5 GeV for fluctuations into or out of that cone as we have seen above. One expects, very crudely, that this error contributes to dM/M a term to be added in quadrature to Eq. 9.

$$(dm/M)_{fluc} = \sqrt{2}\, P_{fluc}/M. \qquad (10)$$

A fixed value of P_{fluc} means that at high masses fluctuations are less important and that the "intrinsic" calorimeter resolution may begin to be the dominant term in the dijet mass resolution. The scale for P_{fluc} to cause a 1% error, dM/M, is estimated to be M = 0.7 TeV in the case that P_{fluc} is caused by fluctuations due to fragmentation and the underlying event.

First one needs to optimize the cone radius defining the jet. In Fig. 7 is shown the standard deviation of the reconstructed to generated dijet mass ratio, δ, as a function of cone radius. If only jet fragments are used, the error decreases smoothly till it reaches a value ~ 0.01 at R ~ 1.0. When the underlying event, and its fluctuations, are added the minimum error occurs at R ~ 0.6. The error is then increased to ~ 2%. This simple clustering algorithm has been checked against a more complete approach.[14] The results given here are stable with respect to the treatment of clustering. Note that in order to contribute to dM/M by 1.4% the scale of momentum fluctuations must be ~ 100 GeV. This size for P_{fluc} is well above the ~ 5 GeV scale which was previously estimated. The origin of this scale for P_{fluc} is "hard" non-colinear gluon radiation and neutrino losses from heavy flavors as will be discussed below in Section 4.

A histogram of the ratio of reconstructed to generated dijet mass is shown in Fig. 8. The bin width is 1%, and the error is 1.3% for the case of R = 0.6 with only dijet fragments used. Note the long "radiative" tail which is due to gluon radiation and neutrinos, as will be discussed later. We assume that this "radiative tail" is soft enough that it cannot be tagged amidst the general debris of the dijet event.

A histogram of the energy of the leading hadronic fragment is given in Fig. 9. Note that the mean $<z_1>$ is 0.26 with a standard deviation of 0.14. These results are consistent with the expectations drawn from consideration of Fig 3.

The result for the mass error as a function of calorimeter depth is shown in Fig. 10. By comparison with Fig. 6 one can see that a purely resolution dominated (Fig. 6) calorimeter with a mass error of ~ 0.7% shifts to a mass error of ~ 2% (resolution and fluctuations) in the case of a very thick calorimeter. The shift in asymptotic resolution means that 10 absorption lengths is more than adequate. The uncertainty is roughly ± 1 unit due to the spread in the data sets. This is an estimate of the extrapolation and systematic errors.

4. Missing P_t and Calorimeter Depth

A signal for the existence of high transverse momentum neutrinos in an event is a large missing transverse momentum. Clearly, this signal can be mimicked by a lack of "hermeticity" caused by holes in coverage at small angles, cracks due to leads or supports, or "leakage" due to inadequate depth of calorimetry. Thus an SSC calorimeter should be deep enough that leakage should not dominate the real sources of neutrinos. A limit to the required depth is provided by the evolution of a gluon jet into a heavy quark pair. The semileptonic decay of either quark provides a source of neutrinos which will "leak" out of the calorimeter undetected. It is in comparison to the scale of this leakage that the scale of calorimeter depth should be evaluated.

4.1 $J \to Q\overline{Q} \to ql\nu$

First, what is the physics source of neutrinos? Obviously there are many. What concerns us here are sources topologically similar to those caused by calorimeter leakage. A gluon jet has a finite probability to vacuum fluctuate into a heavy quark antiquark, $Q\overline{Q}$, pair which then semielectronically decays in the core of a jet.[16] This process acts as an irreducible physics background source of neutrinos in the vicinity of jets. It is assumed that a muonic decay is tagged ($l = \mu$) but that in an electronic decay ($l = e$) the e will be lost in the core of the jet. A rough estimate of the probability is given in Eq. 11. The strong coupling "constant" is taken, for purposes of hand estimates, to be = 0.1. This value is not unreasonable given the mass scales involved and the slow, logarithmic "running" of α_s. The value for the semiloptonic branching ratio, $B(Q \to ql\nu)$ is taken to be 20%.

$$\begin{gathered} \alpha_s / \pi \ln(2M_Q / P_t)\, B(Q \to ql\nu) \\ (P_t)_{miss} \sim P_t / 6. \end{gathered} \tag{11}$$

The cross section for jets, Eq. 5 in arbitrary units, and for the neutrinos, Eq. 11, is shown in Fig. 11. At a fixed P_t, the missing P_t due to neutrinos is down by a factor ~ 10^{-5} with respect to the jet cross section. This factor has 2 components. First, as shown as a vertical dashed line, the probability for $g \to Q\bar{Q}$, $Q \to q\ e\ \nu$ is about 1%. Second, the reduced P_t of the neutrino with respect to the gluon, coupled with the steep gluon P_t spectrum, reduces the cross section by another factor of ~ 1000 at fixed P_t. This six-fold reduction going from P_t to $\not{P}_t$ is shown as the horizontal dashed line in Fig. 11.

4.2 Jet Leakage

In comparison, a calorimeter of finite depth will leak some fraction, 1-f, of its energy out the back. This leakage will cause one to miss some of the energy.

$$\not{P}_t \;=\; (P_t)_{miss} \;\sim\; (1-f)\,P_t. \tag{12}$$

The resulting spectrum for 95% containment is shown in Fig. 11. One obtains it by using the jet cross section and derating P_t by a factor of 20 to get $\not{P}_t$ due to incomplete containment. Clearly, this loss of energy leads to a missing P_t cross section quite comparable to the irreducible rate due to the decays of heavy flavors in jets.

The design criterion is to make the calorimetric leakage < the physics leakage at all accessible (luminosity dependent) dijet masses. An estimate for 10 TeV dijet mass, P_t ~ 5.0 TeV, $k_t \sim \langle z_1 \rangle P_t$, is that ~ 7 ± 1 absorption lengths are needed. Thus the limit on depth placed by the dijet mass resolution appears to be more stringent than that imposed by leakage. Note that this limit has been estimated using only the leading QCD hard $Q\bar{Q}$ fragmentation. It is also true that the response function has been assumed to be a Gaussian characterized by a standard deviation. There are, however, tails which, if not removed, lead to missing transverse momentum which may dominate over real physical processes.[17] We defer discussion of the tails until longitudinal segmentation is discussed.

4.3 Leakage and Calorimeter Resolution

It is interesting to note that the evolution of gluons into heavy flavor fragments places an upper limit on the accuracy of any calorimeter. Thus, one must note that the "leakage' of a jet limits the ultimate "constant term" which one can attain for jets. The probability for a dijet to produce a neutrino can be roughly estimated, in perturbative QCD, from leading fragmentation to be;

$$P(\nu) \sim (4\alpha_s / \pi) \ln(2M_Q / P_t) B(Q \rightarrow ql\nu). \tag{13}$$

For a 10 TeV dijet, P_t = 5.0 TeV, this is ~ 8% for b or c decays into electrons and neutrinos. When that decay occurs, the jet loses ~ 1/6 of its total energy on average or, roughly, 5000 GeV (0.08)/6 = 66 GeV is lost per jet or 1.3%. This loss leads to an error on the jet energy which places a lower limit on the accuracy of energy measurement. The long tail and asymmetric broadening of the mass peak in Fig. 8 is partially due to the presence of neutrinos in the jets.

4.4 Monte Carlo Results

The Monte Carlo program with dijets was used to study the neutrino leakage. A plot of the ratio of the mean leakage energy to the mean neutrino energy for 10 TeV dijets is shown in Fig. 12 as a function of calorimeter depth. At ~ 12 absorption lengths the leakage energy falls below the "intrinsic" leakage due to neutrinos from heavy flavor decays. This result is more restrictive than that which is inferred from Fig. 11, which reflects the effect of an entire chain of fragmentation fluctuations to $Q\bar{Q}$ within the jet. Note that Fig. 11 assumes only "leading" fluctuations.

This cascade effect is displayed in Fig. 13 where the distribution of the fraction of the jet energy possessed by the neutrino is plotted. Most neutrinos are quite soft; the mean energy fraction for all events is 1.6% with a spread of ± 1.4%. However, only 18% of the events have a neutrino, and for these events they carry away approximately 5% of the energy. Clearly, the neutrino leakage effect contributes substantially to the resolution of a thick calorimeter for very high mass dijets.

Assume that the mass error is due to the effects of resolution, fluctuations due to fragmentation and underlying event, neutrino leakage, and depth leakage folded in quadrature. For depths above 10 absorption lengths, the depth leakage is not important. The fluctuation term, Eq. 10, falls as 1/M, and is small for large masses. The effects of stochastic contributions to the energy resolution fall as $1/\sqrt{M}$, Eq. 9, while the neutrino leakage rises as $\ln(M)$, Eq. 13. Finally, the effects of non-colinear gluon emission dominate at high masses.[18] This latter effect has a very soft (logarithmic) decrease with mass. At 10 TeV, the gluon radiation fluctuation is most important, followed by neutrinos, while the energy measurement errors are only third most important.

5. Depth Required for Muon Identification

The calorimeter also serves as a preliminary filter for the muon identification system. Clearly, one should examine whether the total depth of the calorimeter is also sufficient for this task. The total depth of the muon system is set by global considerations for muon identification.[19] The calorimeter depth should be sufficient to insure that the rate from hadronic punchthrough is less than the irreducible rate from pion decays in the tracking volume. In order to explore this criterion, the source of pions was taken from CDF data for transverse momenta, P_t, below 10 GeV.[20] The cross section was scaled up to give a rapidity space density of 8 particles per unit of y. The resulting rate, at SSC design luminosity, at $y = 0$, for pion decays into muons, with a 2m decay radius, is shown as a function of P_t in Fig. 14a. Clearly, after 10 absorption lengths, the rate integrating over all P_t is roughly 10^5 Hz per unit of rapidity.

The pions from minbias events also occasionally punchthrough the calorimeter into the region occupied by the inner muon detectors. The rate of punchthrough is estimated using a parameterization of the WA1 data.[21] The rates for punchthrough are given in Fig. 14b, along with the pion decay rate. Clearly, real muons dominate over punchthroughs for a calorimeter thickness > 7 absorption lengths. Since this thickness is less than that which has already been considered on the basis of resolution and leakage studies, one concludes that no more stringent requirement appears to be imposed by considerations of the muon system.

6. Longitudinal Segmentation and Depth

6.1 Energy Asymmetry and Resolution

Until now the calorimeter has been considered to be a unitary object. However, at some point the fact that the cost of materials scales as D^3 means that depth segmentation may become an attractive alternative to adding more depth. In the context of the WA1 model (Section 2.2), dividing a D = 10 calorimeter into D1 = 6 and D2 = 4 segments allows one to measure the interaction point and therefore estimate and/or tag the leakage.

The interaction point is determined, on average, by the energy asymmetry δ which is correlated with the energy leakage fraction γ:

$$\begin{aligned} \delta &= (E_1 - E_2)/(E_1 + E_2) \\ \gamma &= E_L/E. \end{aligned} \tag{14}$$

A plot of the numerical results for the mean values of δ and γ at representative energies and interaction points is given in Fig. 15. The form of Eq. 2 was used, but the additional smearing due to the fluctuation in shower shapes, dfo (Eq. 3), was not put in. The relationship is sufficiently well parameterized by the form

$$\begin{aligned} \delta &= 1.0 - \gamma/\gamma_{EFF} \\ 1/\gamma_{EFF} &= 4.2\ (1 - 0.095 \ln E). \end{aligned} \tag{15}$$

Clearly, in the absence of any other fluctuations in the shower, the energy leakage can be corrected for using the depth segmentation. This correction should improve the energy resolution by correcting for the interaction point smearing (see Eq. 3).

The containment and resolution of a D = 10.1 calorimeter longitudinally segmented into D1 = 6.6 and D2 = 3.5 were studied using the Lab E data. Representative data are shown in Fig. 16. In Fig. 16a is shown the distribution of containment fractions, f, for 450 GeV beam incident on the calorimeter. Note the long tail caused by fluctuations in the hadronic shower development. These fluctuations defeat attempts to use the energy asymmetry δ to make the calorimeter thinner while preserving the resolution. It was found that no improvement in the Gaussian part of the resolution could be obtained using information from the two depth segments.

6.2 Back Section Veto and Containment

The non-Gaussian tails in the resolution due to fluctuations can still be reduced. In Fig. 16b, is shown the same distribution except that the cut on Δ, the ratio of D2 energy to total incident energy, $\Delta < 0.18$, was made. Clearly, the long tail is much reduced while preserving the events in the f $\simeq$ 1 region with good efficiency. The cut passed ~ 85% of all events. Harder cuts on Δ improved the containment fraction average.

The segmentation studies were then extended to cover different energies and total depths. After some inspection of the events it was decided to keep a D2 = 3.5 depth back segment. The reason for this is that the low f hadronic showers often appear "disconnected" with initial clumps of energy, a gap, and then a second energy clump. The width of these gaps roughly dictates the value of D2.

In Fig. 17a is shown the efficiency for events as a function of Δ. The efficiency fails roughly logarithmically with the cut. At a fixed depth, D, the efficiency falls with energy at fixed Δ as expected since showers penetrate deeper into the calorimeter with increasing energy. At fixed energy the efficiency at fixed Δ falls as the total calorimeter depth is decreased.

The fraction of events, F, with less than 95% containment as a function of Δ is shown in Fig. 17b. At an energy of 450 GeV, using the resolution that has been assumed so far ($dE/E = 0.5/\sqrt{E} \oplus 0.03$) the error is $dE/E = 0.038$ which sets a scale which should be comparable to F. This fraction, F, falls as a power of Δ as one expects since that is the purpose of the Δ cut. It also rises with energy at fixed Δ, as expected. At fixed Δ, F rises as D decreases since a thinner calorimeter will leak more.

Comparing the Figures, one can establish the tradeoffs. First, some longitudinal segmentation cut is needed in order to control the tails lest the real missing transverse momentum signal due to neutrinos be swamped by leaking hadrons.[17] Second, can the calorimeter be made thinner to save costs? As shown above, for $D < 10$, a thinner calorimeter degrades jet energy measurements at the highest accessible jet energies. Third, the fluctuation tail can be controlled with a thinner calorimeter, but at the cost of an inefficiency. For example, if F = 0.05, i.e., 95% containment for 95% of the events, then for 450 GeV, $\Delta = 0.36$ for $D = 10$ with $\epsilon = 1.0$ while $\Delta = 0.14$ for $D = 8.7$ with $\epsilon = 0.5$. Since 450

GeV corresponds to $z \sim 0.09$ for a 10 TeV dijet, which is $< z_1$, one expects that the rare high-mass dijets will be vetoed by the leakage cut on Δ leading to a large inefficiency if $D < 10$.

7. Summary and Conclusions

The requirements of SSC Physics on calorimeter depths were studied. First an ensemble of data sets at energies < 450 GeV were assembled and parametrized. This ensemble, when extrapolated to SSC energies, indicates the range of systematic errors.

The Physics process which was chosen was dijets at the highest accessible (rate limited) mass, M = 10 TeV. The leading fragment in such an event has $z_1 \sim 0.2$ or $k \sim 1$ TeV. Using the parametrizations, one finds that $D(y = 3)/D(y = 0) = 1.2$. Only a 20% increase in thickness is needed as pseudorapidity goes from zero to three.

A Monte Carlo study of the dijet mass resolution indicated $dM/M \sim 2\%$ for $D > 10$. For thinner calorimeters, the Gaussian part of the resolution was increased due to leakage errors. The dijet mass resolution was found to depend mostly on fragmentation fluctuations, which reduced the sensitivity of dM to calorimeter resolution and leakage effects.

Neutrinos from $Q\bar{Q}$ pairs which evolve in the jet begin to become important for dM at the highest masses. Defining the criterion to be that missing P_t due to leakage be less than missing P_t due to neutrinos in jets leads to the requirement $D < 11$.

The calorimeter also removes hadrons as the front filter for the muon system. Defining the criterion to be that the rate behind the calorimeter due to punchthrough (leakage) be less than the rate due to pion decays in a 2 m radius upstream of the calorimeter leads to the requirement $D < 7$.

Longitudinal segmentation was found not to be useful in improving resolutions. However, it is extremely useful in vetoing the long tail in the resolution corresponding to poor containment/large leakages. A cut of $\Delta = 0.18$ effectively removes the non-Gaussian leakage tail for energies < 450 GeV in that the fraction with 95% energy containment is = 97% (450 GeV), > 98% (< 100

GeV), if D = 10. The loss of real events with this cut is < 15% for E < 450 GeV.

In conclusion, given a systematic error spread due to the extrapolation of existing data, a calorimeter with depth D = 10 segmented into D1 = 6.5, D2 = 3.5 will not degrade jet measurements, muon systems, or missing transverse momentum measurements at the SSC.

Acknowledgments

The fine efforts and great patience displayed by Ms. S. Weber and Ms. T. Gourlay are most greatfully acknowledged by the authors.

REFERENCES

[1]F.J. Sciulli, Photon-Collecting Hadron Calorimeters, presented at the *Calorimeter Workshop*, May 8 & 9, 1975, Fermilab.

[2]S. Iwata, preprint, DPNU-3-79, February 1979, Nagoya Japan.

[3]M. Holder, Nuc. Inst. Meth. 108, 54 (1978).

[4]K. Rauschnabel, preprint, KEK-EXT 3/78-5.

[5]D.L. Cheshire, Nuc. Inst. Meth. 126, 253 (1975).

[6]R.K. Bock, Nuc. Inst. Meth. 186, 533 (1981).

[7]E. Hughes, "Study of Hadronic and Electromagnetic Shower Development between 10 and 140 GeV by an Iron-Scintillator Calorimeter." In *Proceedings of the First International Conference on Calorimetry in High Energy Physics*, edited by D.F. Anderson, M. Derrick, H.E. Fisk, A. Para, and C.M. Sazama, pp. 525-538. Singapore: World Scientific Publishing Co. Pte. Ltd., (1991).

[8]F.J. Sciulli et al., Unpublished data from hadron test beam exposures of the full sized neutrino detector. The detector dimensions insure negligible transverse or longitudinal leakage in distinction to other test modules. W.K. Sakumoto et al., Nuc. Inst. Meth. A294, 179, (1990).

[9]J.F. Owens et al., *Design and Utilization of the SSC, proceedings of, Snowmass 1984*, 218 (1984).

[10]D. Green, *PP Collider Physics*, FNAL-CONF 89/70.

[11]D. Green, *Dijet Spectroscopy at High Luminosity*, FNAL-CONF-90/151.

[12]Review of Particle Properties, Phys. Lett B, 239 1-516 (1990).

[13]R. Plunkett and F. Abe et al., *Jet Dynamics at the Tevatron Collider*, FNAL-Conf-89/261-E, Phys. Rev. Lett. 65, 968 (1990).

[14]W. Wu., "Results from Clustering Method for High Pt Z Jets," SSC-SDC-F60, and "Results from Clustering Method for Low Pt Z Jets," SSC-SDC-F63, Fermilab SDC Internal Notes (1990).

[15]A. Beretvas et al., "SSCSIM User's Guide," SSC-SDC-F31, Fermilab SDC Internal Notes (1990).

[16]R.K. Ellis, *An Introduction to the QCD Parton Model*, FNAL-CONF-88/60-T.

[17]J. Hauptman, and M.Y. Pang, "Hermeticity Study Using the CCFR Data," SDC-89-00011, SSC Solenoidal Detector Internal Note, September 15, 1989.

[18]G. Sterman and S. Weinberg, Phys. Rev. Lett. 39, 1436 (1977).

[19]D. Green and D. Hedin, Nuc. Inst. Meth. A297, 111-120 (1990).

[20]F. Abe et al., Phys. Rev. Lett. 61, 1819 (1988).

[21]D. Green, "Muon Triggering at Small Angels." In *Proceeding of the Workshop on Triggering, Data Acquistion, and Computing for High Energy/High Luminosity Hadron-Hadron Coliders,* edited by B. Cox, R. Fenner, and P. Hale, pp. 402-408. Batavia: Fermi National Accelerator Laboratory (1985).

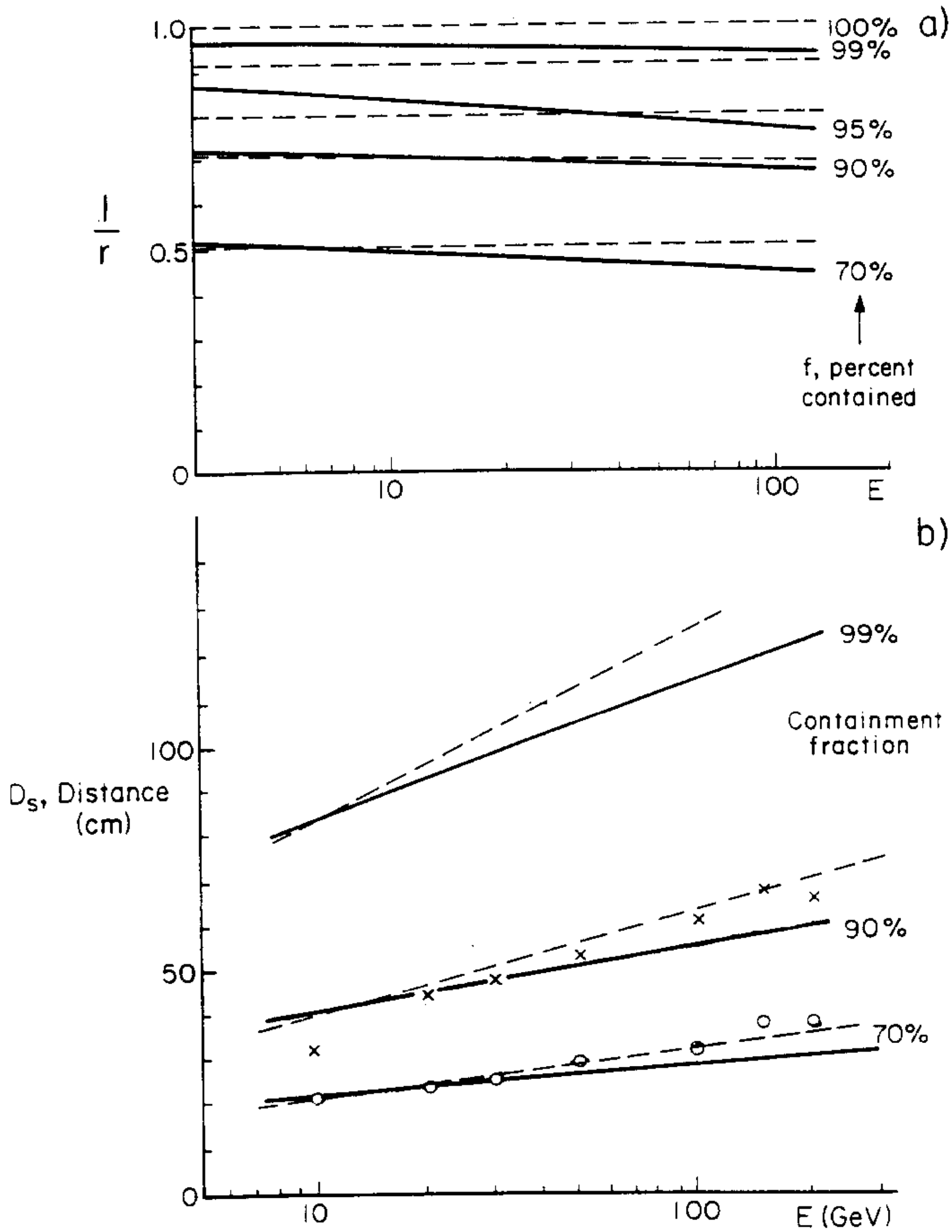

1. Dashed curves refer to the parameterization described in the text. Solid curves refer to a model described in Ref. 1.

    a. Resolution ratio as a function of energy for several energy containment fractions, f.

    b. Distance in steel required for a given energy containment fraction as a function of energy for 3 values of f.

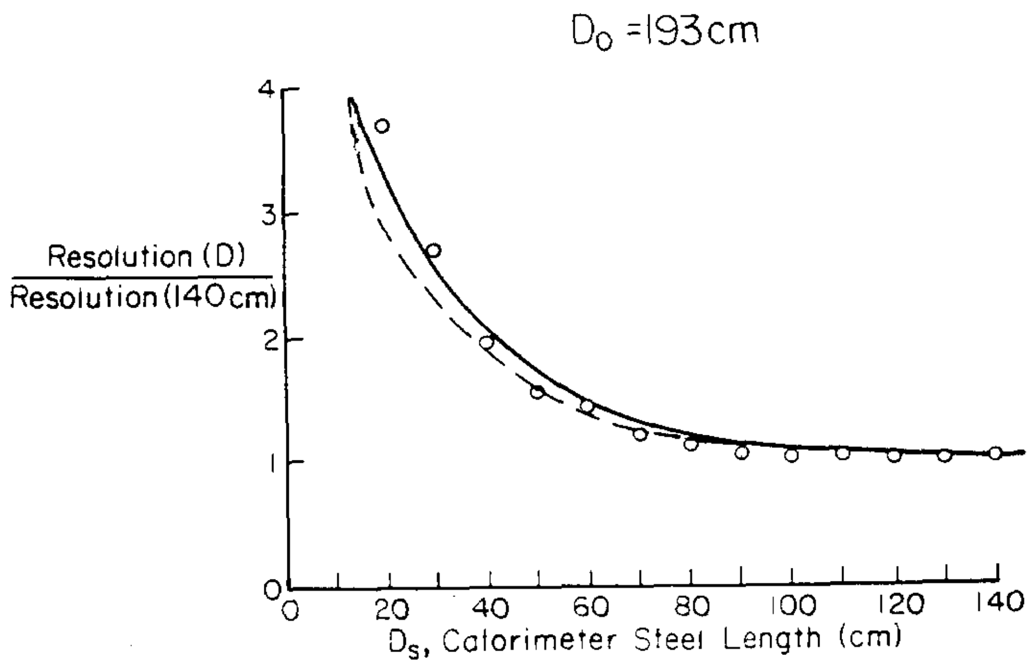

2. Resolution ratio with respect to total thickness at fixed energy, 200 GeV, as a function of calorimeter depth. Dashed curve is a parameterization as described in the text.

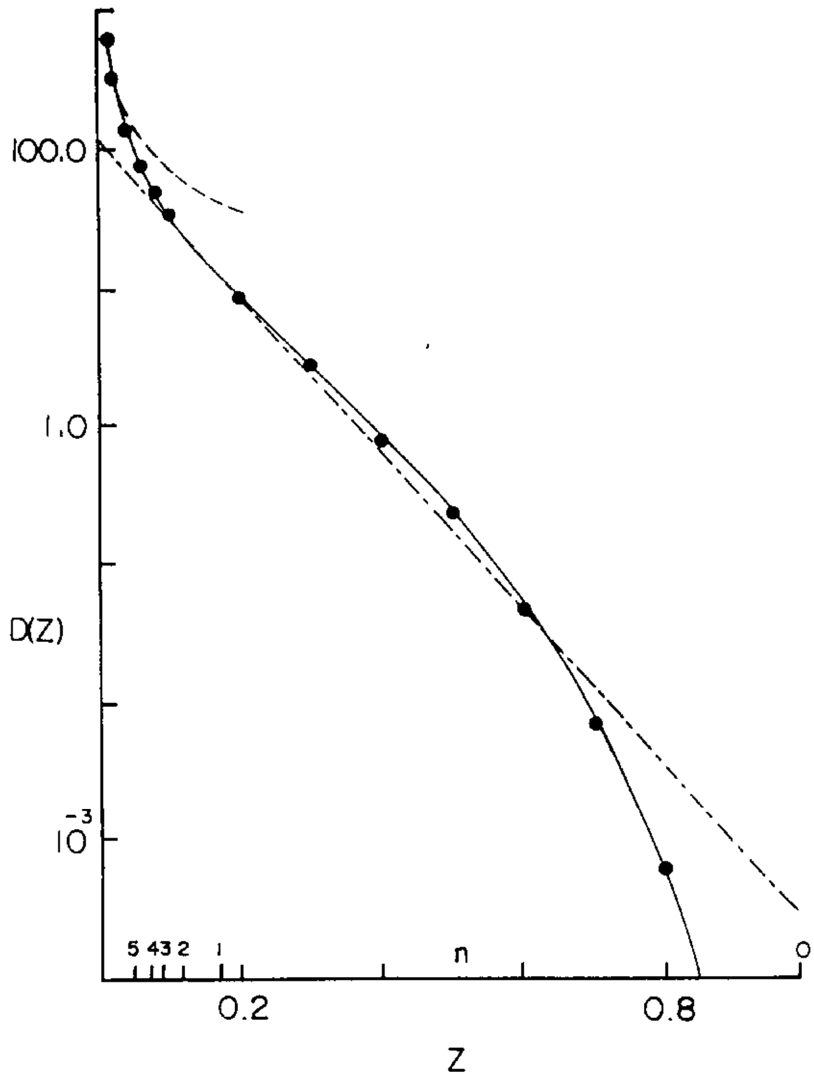

3. Fragmentation function D(z) as a function of z. The points are taken from Eq. 6., while the dashed and dashed-dotted curves are approximate forms which are discussed in the text. Also indicated are the z values appropriate to multiplicities 1 through 5.

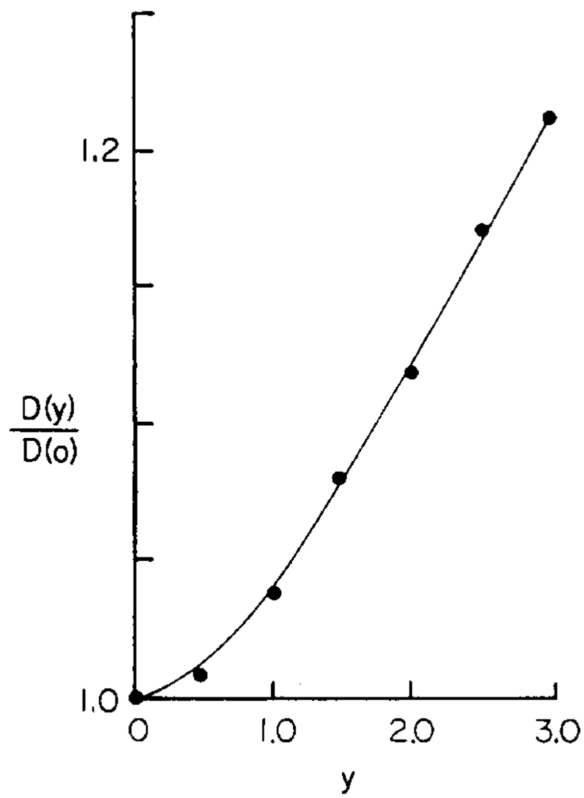

4. Ratio of depths required at y = 0 and at variable y as a function of y for a 10 TeV dijet mass.

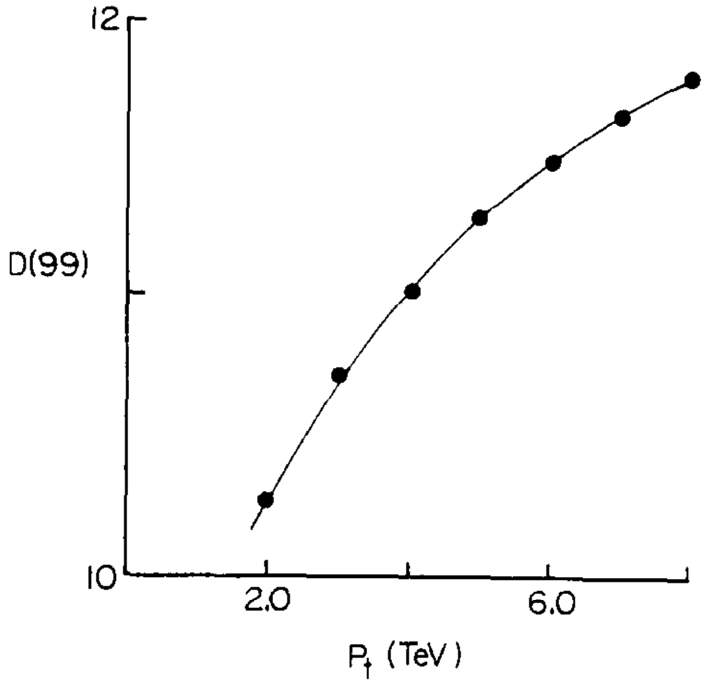

5. Required calorimeter depth, in steel absorption length units, to achieve f = 0.99 as a function of the P_t of the jet.

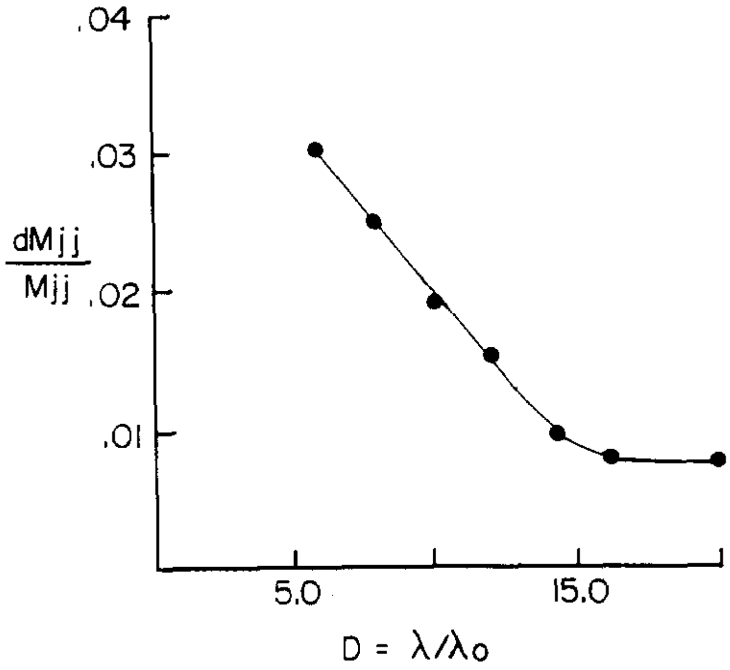

6. Fractional dijet mass resolution for a 10 TeV dijet mass as a function of calorimeter depth. Note that the resolution at great depths is only that due to energy resolution of the jets; fluctuations in fragmentation and the underlying event have not been included.

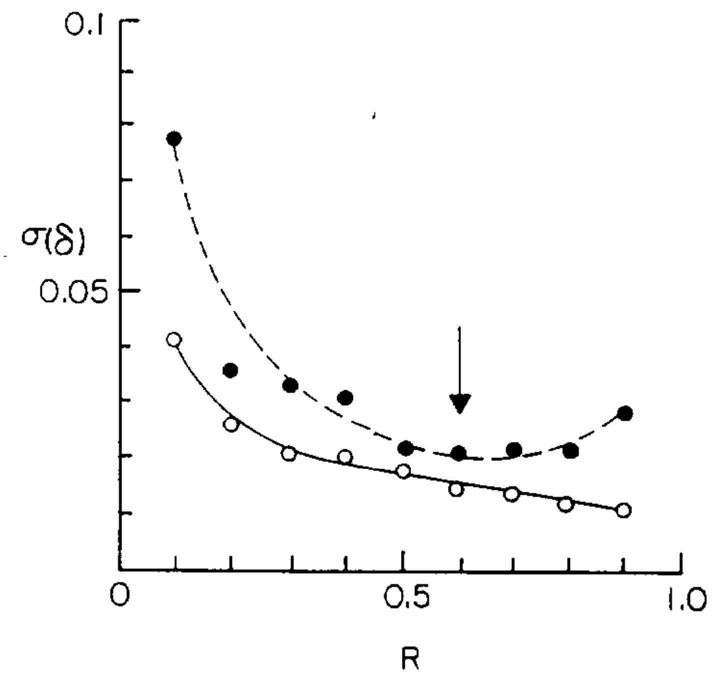

7. Standard deviation of the ratio of the reconstructed to generated dijet mass for 10 TeV dijets as a function of containment cone radius R. The points, o, refer to the case where only jet fragments are used. The points, •, refer to the case where all particles in the event are used if they fall within the cone.

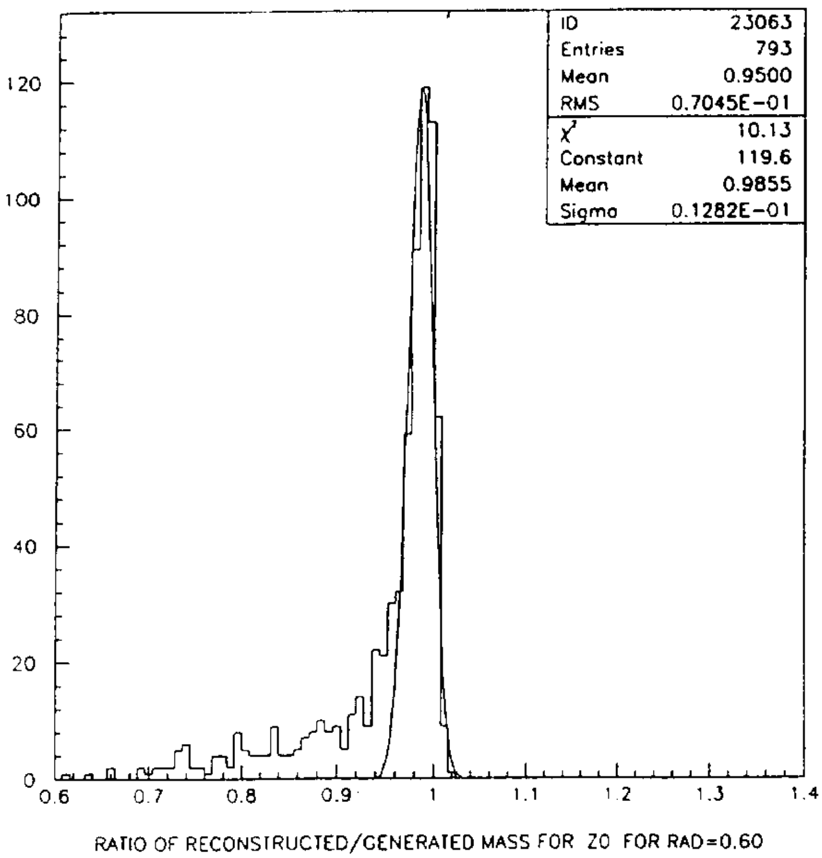

8. Histogram of the ratio of reconstructed to generated mass for 10 TeV dijets using a cone of radius R = 0.6. Only jet fragments are used in the calculation.

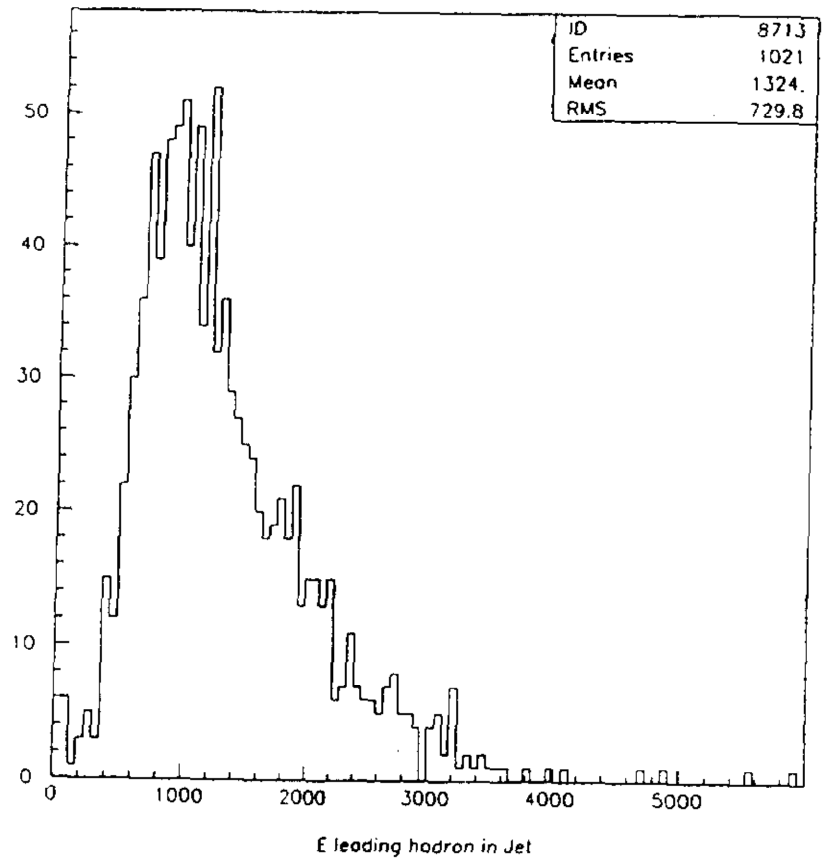

9. Histogram of the energy of the "leading" hadronic fragment for a *10* TeV dijet. The energy units are GeV.

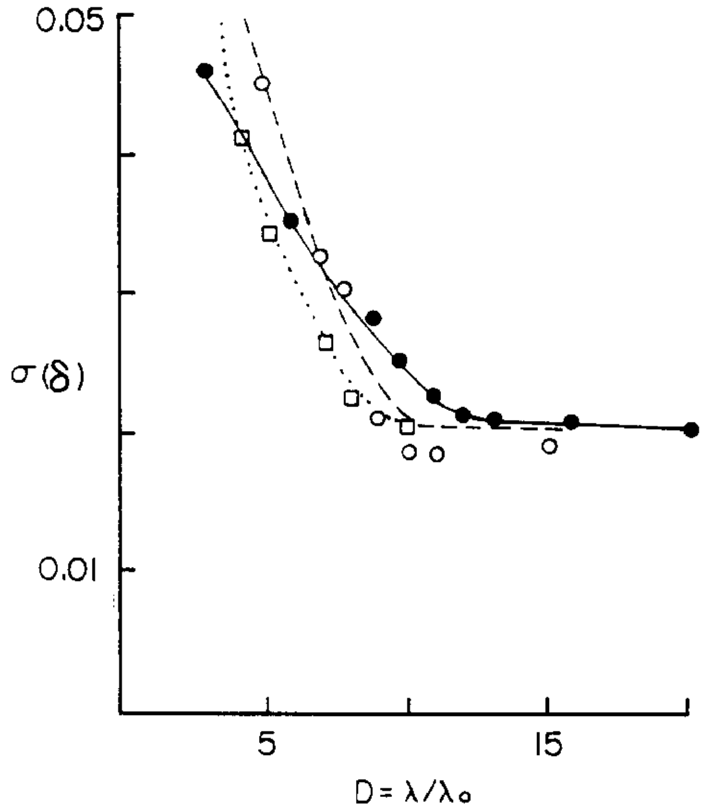

10. Error on the ratio of reconstructed to generated dijet mass as a function of the depth of the calorimetry for 10 TeV dijets; CITF •, WA1 o, Lab E,□, parametrizations.

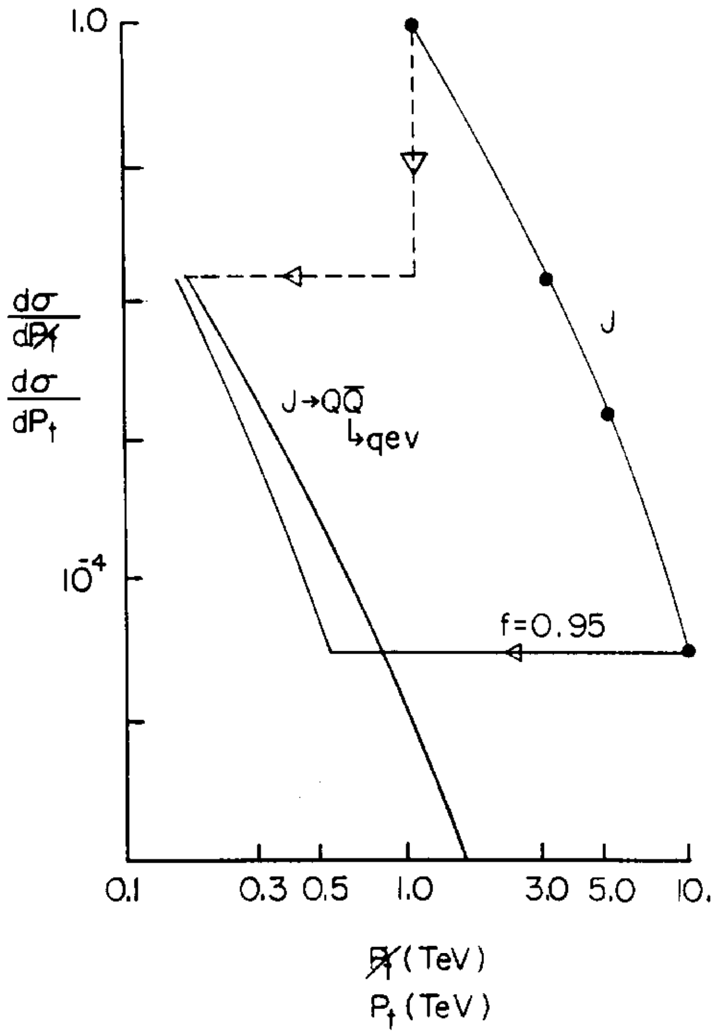

11. Cross section (arbitrary units) for missing P_t due to jets. For jets, the horizontal axis is the jet transverse momentum, P_t. The two possibilities which are shown are semileptonic decays of heavy quarks from leading fragments of gluons and leakage of jet fragments due to finite calorimeter depth.

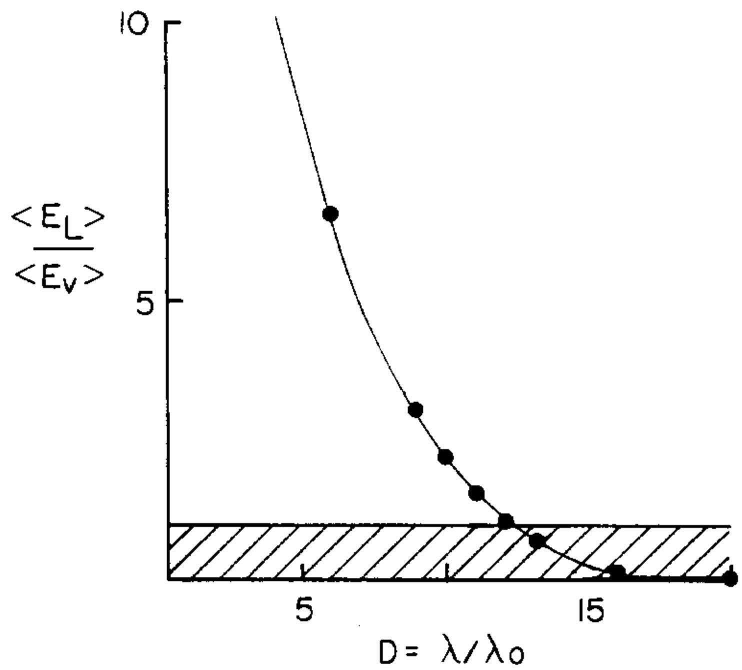

12. Ratio of mean leakage energy to mean neutrino energy as a function of the calorimeter depth. The hatched region corresponds to "leakage" dominated by neutrinos.

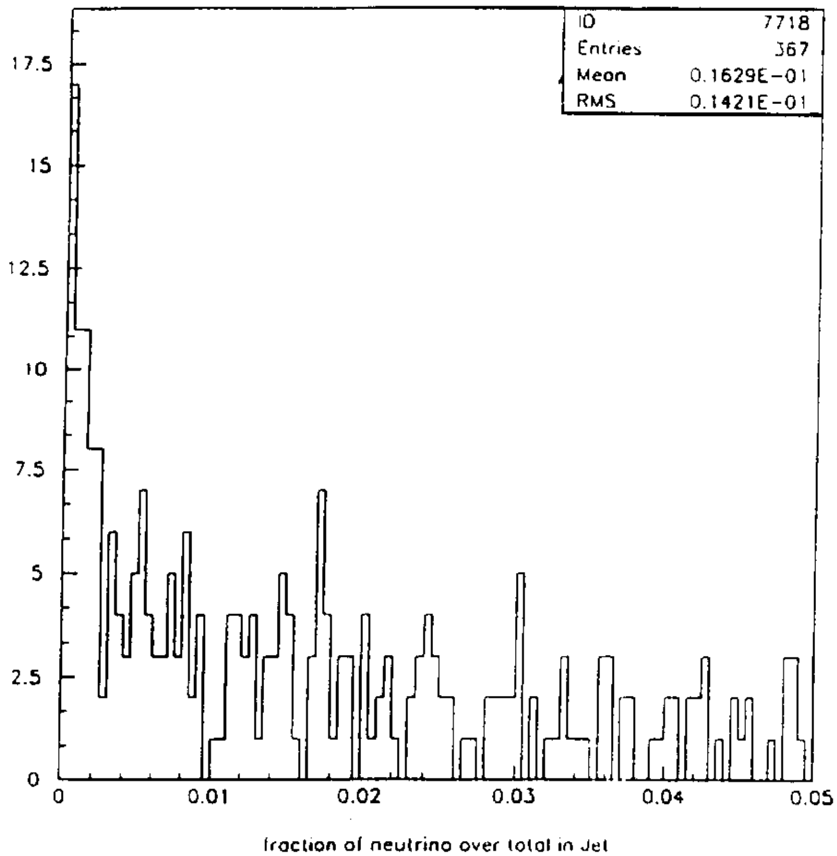

13. Histogram of the fraction of the jet energy carried away by neutrinos. For leading fragmentation this fraction would be equal to 1/6.

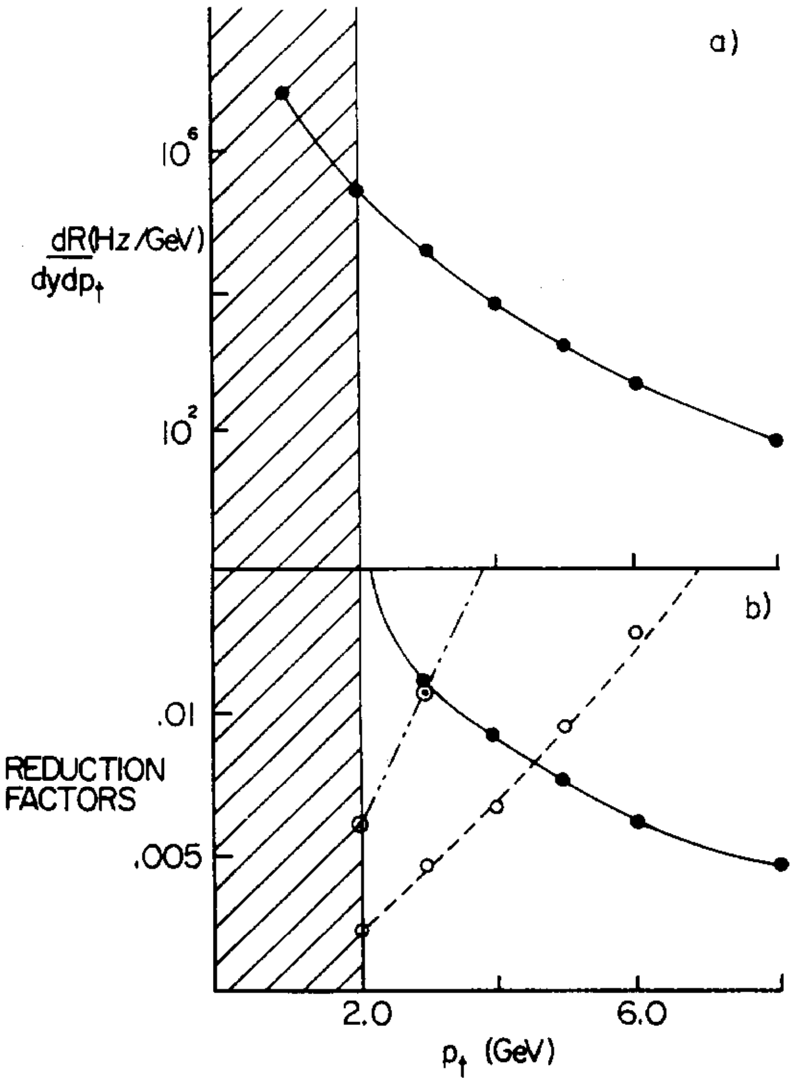

14. Rates behind the calorimeter germane to muon detection.

    a. Rate for muon decays as a function of P_t at $y = 0$. The shaded area corresponds to the range cut of 10 absorption lengths of steel.

    b. Reduction factors with respect to pion rates for decay muons, •, punchthrough at 7 absorption lengths, ⊙, and at 8 absorption lengths, o, as a function of P_t at $y = 0$.

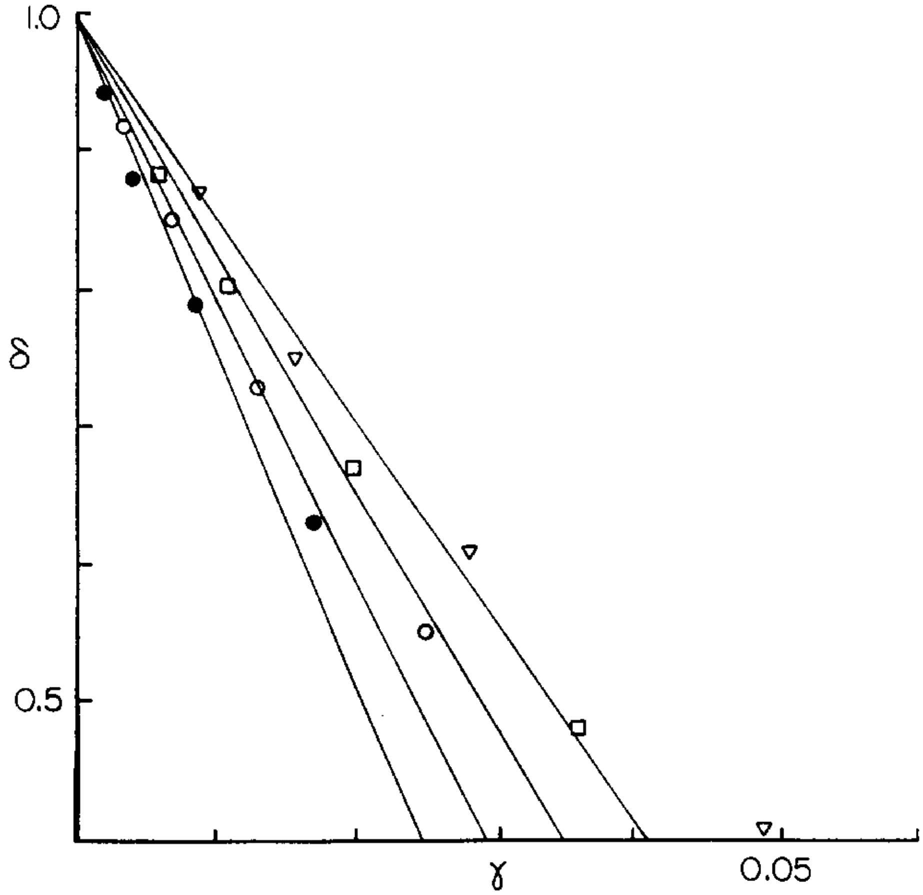

15. Energy depth asymmetry, δ, calculated using the WA1 parametrization as a function of leakage ratio, γ, for various energies; 100, 200, 400, 800 GeV corresponding to •, o, □ , and ▽ , respectively. The calorimeter depths are D = 10, D1 = 6, and D2 = 4. The electromagnetic fraction, fo, is fixed at the WA1 value.

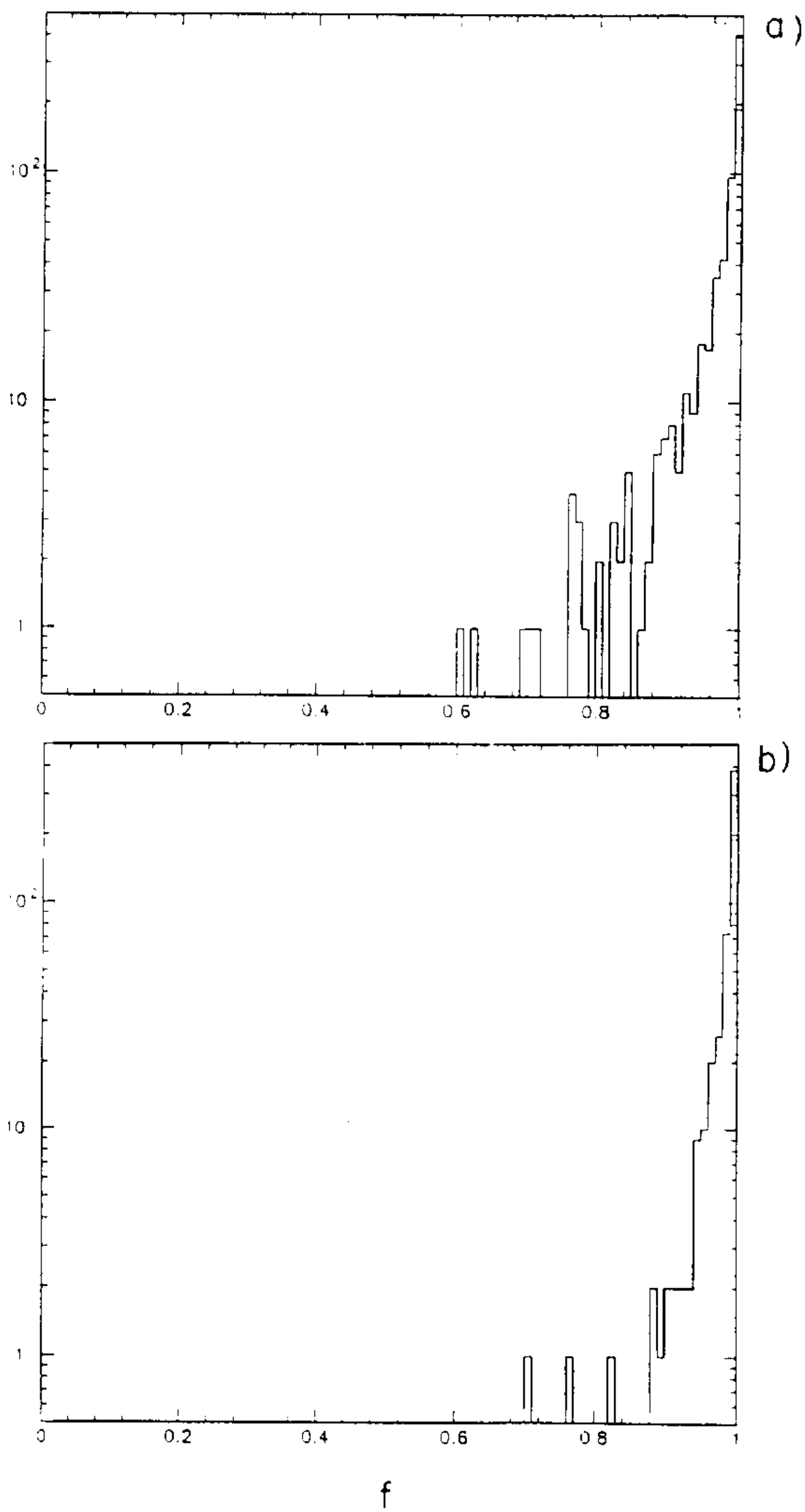

16. The distribution, for 1000 events, of the containment fraction f for 450 GeV incident beam.

   a. D = 10.1 calorimeter, no longitudinal segmentation.

   b. D = 10.1 calorimeter with D1 = 6.6 and D2 = 3.5 longitudinal segmentation. The fractional beam energy, Δ, in the back, D2, segment must be < 0.18.

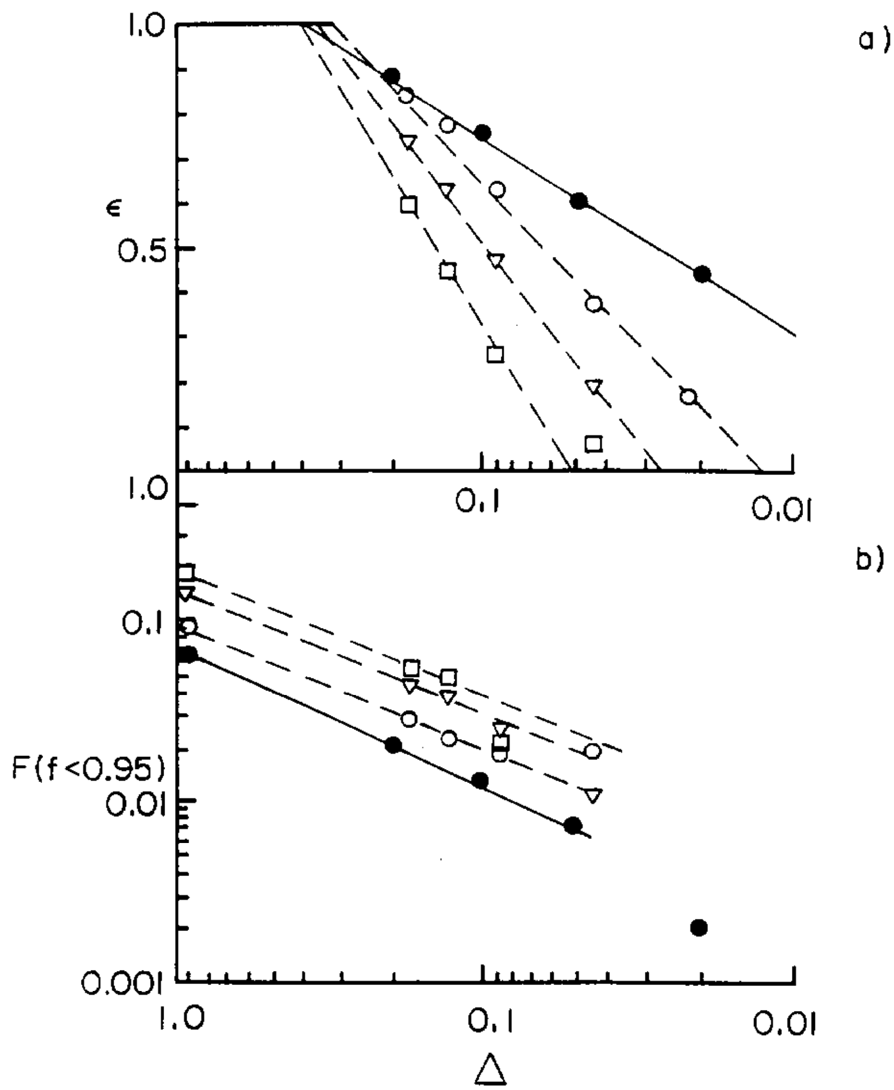

17. In this Figure lines are drawn to guide the eye. Solid lines refer to 100 GeV data while dashed lines refer to 450 GeV data. The meaning of the symbols is that:

• = 100 GeV, D = 10.1, D1 = 6.6, D2 = 3.5
o = 450 GeV, D = 10.1, D1 = 6.6, D2 = 3.5
∇ = 450 GeV, D = 9.4, D1 = 5.9, D2 = 3.5
□ = 450 GeV, D = 8.7, D1 = 5.2, D2 = 3.5

a. Efficiency of event acceptance as a function of Δ, the fractional beam energy cut in the back segment.

b. Fraction of events, F, with containment fraction, f, < 95% as a function of Δ.